MANAGING PUBLIC TRANSIT IN THE PREVALENCE OF PANDEMIC AND REOPENING THE ECONOMY

Word Count: 7193 words + 1 table(s) × 250 = 7443 words

Submission Date: August 1, 2020

ABSTRACT

As the COVID-19 pandemic is rapidly evolving globally, public transit keeps playing a pivotal role in satisfying the essential workers' demand for commuting and paves the way for reopening the economy. Local transportation agencies face a health-and-economics trade-off when developing context-specific operation plans for public transit. Without strategic preparedness, mass transit facilities are potential hotbeds for the spreading of infectious diseases. This work provides a network-based analysis for this trade-off by computing the maximal commute network flow with strict public health measure constraints. The resulting plans include the traffic flow restrictions imposed on each route and are adaptive to the time-varying epidemic dynamics. A case study during the COVID-19 pandemic shows that the properly planned subway system in New York City can maintain 88% of traffic while reducing 50% of the risk of disease transmission compared with fully-loaded public transit services. Transport policy-makers can exploit this optimization-based framework to resolve the health-and-economic trade-off and make proactive reopening plans.

Keywords: Public transit, Spatial compartmental model, Health-and-economics trade-off

INTRODUCTION

Operating public transit amid post-peak and post-pandemic periods is a double-edged sword: on the one hand, it provides basic and low-cost mobility services to those not owning cars or who place environmental concerns at the center of commuting decisions; on the other hand, human mobility, especially commuting by mass transit, contributes to the spatial propagation of infectious disease. Policy-makers face this *health-and-economics* trade-off when lifting the restrictions and restarting public transit systems during the unprecedented COVID-19 pandemic. There is attainable evidence (*1, 2*) that the pandemic outbreak had a disproportional impact on mass transit operators and passengers compared with other groups of the population. Due to safety concerns, many countries have implemented the closure of transit systems (*3*); in some countries, ridership of public transit has dropped up to 90% (*4, 5*). While the potential risk of epidemic exposure inside subway carriages or buses has been well-recognized (*6*), there is a lack of scientific knowledge about the corresponding prevention strategies. This work aims to answer a critical question frequently raised by transportation agencies and researchers: How to control the traffic flows in the public transit networks to assist the safety preparedness in the period of infectiousness?

To answer this question, we first model the spread and mitigation of a particular epidemic disease through public transit networks by a metapopulation model. The risk of disease transmission associated with public transit depends on the characteristics of the disease and the intervention policies implemented in the workplace and the trip to work (Figure 1). Next, we outline a mathematical-programming approach to develop responsive public transit policies for the evolving epidemics with the interplay of these factors. By applying targeted interventions on high-risk transit routes and regions, most inelastic travel demand is satisfied while the spatial propagation of the infectious disease is restrained.

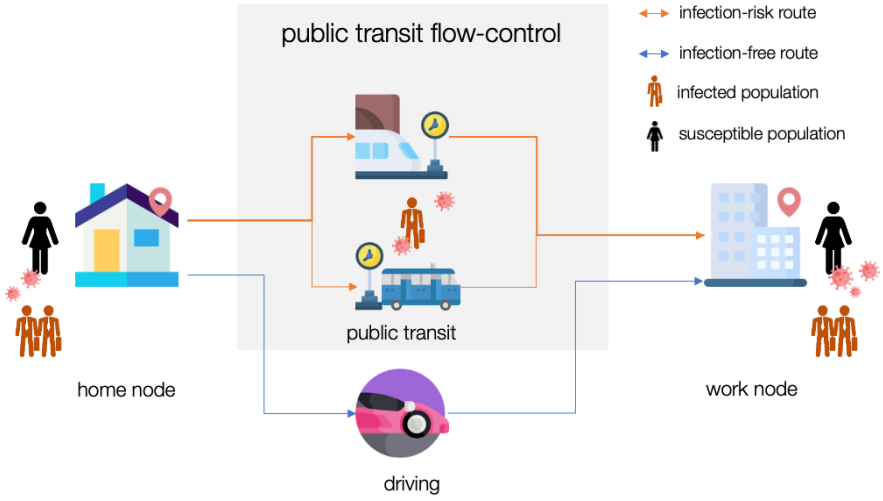

FIGURE 1: Illustration of public transit interventions under the pandemic; arrows mean round-trips for daily commuting.

Related work

There is a resurgence of interest in modeling the disease contagion processes mediated by recurring commuting trips. The development of advanced metapopulation network models coincides

with the pattern of increasingly frequent epidemics in recent years. Keeling et al. (*7*) initiated the stream of network models for the spatial spreading of infectious disease in the commuter-to-work networks. They addressed the fact that the infection dynamics in the recurrent commute networks were significantly different from their counterparts in the kernel and random mobility networks. A similar conclusion was drawn in (*8*), whereas the diffusion rate and recurrent commuting rate jointly determine whether or not the global spreading of the infectious disease occurs. Bichara and Iggidr (*9*) analyzed how the heterogeneous groups, patches, and mobility patterns affect the disease prevalence by a multi-group compartment model. Since the individual's commuting patterns are no longer random, Yashima and Sasaki (*10*) found that the commute networks' topological characteristics such as the networks' degree distribution become relevant. When the degree of networks follows a heavy-tailed distribution, the disease invasion threshold decreases significantly. Hence, the epidemic is not preventable by merely random interventions such as quarantine and vaccination. Therefore, studying the relationship between commute networks and disease dynamics is of interest to epidemiology and transportation research.

A vast body of literature has extensively investigated transportation networks' operations after disruptions (e.g., natural disasters) and incidents such as strikes and epidemics as in this work. As transportation systems are essential for the functioning of cities after disruptions, their resilience has become a key design principle (*11*). This stream of work centers around enhancing the networks' ability to maintain operations during the disruptive period or minimize the required resources for recovery. Note that the enhancement of transportation networks' resilience is only a derivative of measurements in previous work.

In an attempt to identify the risk of taking public transit during the outbreak of COVID-19, an infectious disease with millions of confirmed cases globally, Mo et al. (*12*) proposed an individual encounter model that characterizes the transmission of the disease on public transportation facilities. As an agent-based model, the encounter model captures the probability of contact between each individual and thus evaluates the risk of transmitting a disease from an infectious person to a susceptible one. They calibrated the model using the smart card data from Singapore. Using a similar approach, Qian et al. (*13*) conducted a cross-city comparison of the contact networks using the smart card data from China. They constructed a universal generation model to explain the correlation between the metro contact network's properties and the risk level of transmissible diseases. Note these prior work all use the contact networks as the epidemic model to capture the social activity contacts; thus, rich trajectory data is required for model fitting. More importantly, these models only studied the spreading of the infectious disease in transit ignoring the interactions between commuters and other population. Considering the short period of commuting compared with other activities during the day, separating these two population seriously underestimate the value of public transit intervention policies. Chang et al. (*14*) combined the metapopulation model and commute networks to explain why the infection rates among disadvantaged groups were higher than the rest. Compared to agent-based models such as the individual encounter model, metapopulation models requires access to demographic survey data that is normally publicly available.

While previous research typically only investigated the descriptive and predictive models , this work proceeds to develop a prescriptive model for transit networks. Blending the advances in the metapopulation epidemic models with the network fortification models, the resulting optimization lays the foundation for making transportation policy that balances the need for returning to normal activities and the prevention of public health hazards.

Objectives and main contributions

This work focuses on optimizing the commute networks' operations under disruptions caused by emerging infectious diseases. We are specifically interested in controlling the mobility patterns with dual objectives – providing reliable access to public transit services while slowing the communicable disease invasion.

The main contributions of this work are:

1. Developing an optimization-based analysis by integrating the spatial epidemic model and the commute network model.
2. Providing an iterative method to solve the large-scale transit traffic control policies and obtain general insight for effective interventions.
3. Investigating the optimal subway route operations plans in Manhattan, New York City (NYC) and evaluating the impact on the transmission of COVID-19 pandemic.

Note that the method developed in this work can be applied to any infectious disease that can be potentially transmitted by using public transit services, e.g., with a mix of aerosol and contact transmissions inside vehicles. The spatial epidemic model on the commute networks captures the influence of two most common and effective regulations: *quarantine* policies (population with severe symptoms is forced to stay at home) and *social-distancing* policies on public transit. Our work is a first attempt to investigate the adaptive transit traffic control policies considering the joint effects of repetitive commuting patterns and epidemic dynamics. The model developed in this work requires access to only publicly-available data and thus can be easily adopted by local transportation agencies to make data-driven responsiveness and preparedness plans.

METHOD

Metapopulation model for commute networks

This work focuses on the recurring commuting trips, which account for 79% of all transit trips in the United States (including work and school trips) (*15*). Commuting remains the primary demand for traveling during the epidemic period and revives rapidly in the reopening of the economy (*16*).

Three main approaches for modeling the commute mobility patterns have been used in the past. First, we may model the movement in urban commute networks on the individual level. However, reconstructing the contact networks is not possible without access to massive human motion trajectory data (*12*). Tracking passengers' use of public transit and alternative modes is costly and slow in implementation, occasionally impossible due to privacy concerns, and biased due to limited users of electronic devices. The second approach for modeling traveling patterns is random mobility models. Nevertheless, prior work has revealed that recurring commute trips (i.e., individuals take the fixed routes back and forth) have a significant impact on the disease dynamics and the derived control policies (*7*). Therefore, modeling heterogeneous mobility patterns is critical for developing safe and effective public transport policy.

A promising alternative option is the metapopulation model for the following reasons. First, conventional transportation planning has been using basic geography units such as traffic analysis zones (TAZ) or census tracts, so there is a rich literature on the fundamental methodology and datasets in the hands of local transportation agencies. Second, leveraging the richness of urban planning and transportation models associated with these basic geography units, researchers can explore the connections to commuters' demographical features to develop context-specific plans in preventing epidemics. Finally, epidemic response policies and guidance are often made on a macroscopic network level. In what follows, we introduce how to construct such a metapopulation

model for commute networks.

During the day, each resident is in one of three statuses: at home ("H"), at work ("W"), or commuting ("C"). The underlying *commute network* integrates two separate systems: a home-and-work network $(\mathscr{V}_{HW}, \mathscr{E}_{HW})$ consisting of basic geography units such as census tracts or TAZs, and public transit networks $(\mathscr{V}_C, \mathscr{E}_C)$ serving daily commute between home-and-work nodes.

1. Home-and-work network:
   (a) Residents live in a closed complete network with a fixed population $N_v \in \mathbb{Z}^+, v \in \mathscr{V}_{HW}$. We denote $N = [N_v]_{v\in\mathscr{V}_{HW}}$ whenever there is no possibility of confusion.
   (b) Each vertex $v \in \mathscr{V}_{HW}$ has a set of neighboring outflow vertices $\mathscr{N}^+(v) := \{u \in \mathscr{V}_{HW} : (v,u) \in \mathscr{E}_{HW}\}$ and a set of inflow vertices $\mathscr{N}^-(v) := \{u \in \mathscr{V}_{HW} : (u,v) \in \mathscr{E}_{HW}\}$. The fraction of residents at v travels to $u \in \mathscr{N}^+(v)$ is $r_{vu} \in [0,1]$. The conservation law ensures that the fractions satisfies $\sum_{u\in\mathscr{N}^+(v)} r_{vu} = 1$ for all $v \in \mathscr{V}_{HW}$.
2. Public transit network:
   (a) A set of vertices $\mathscr{V}_C$ represents the public transit routes available in the region, where each *route* may contain transfers between multiple modes or lines.
   (b) Expanding $\mathscr{V} = \mathscr{V}_{HW} \cup \mathscr{V}_C$ such that each region $v \in \mathscr{V}_{HW}$ is connected to reachable routes through edges $\mathscr{E}_C$.
   (c) We define the outflow and inflow to public transit as $\mathscr{C}^+(v)$ and $\mathscr{C}^-(v)$, respectively, upon edges $\mathscr{E}_C$. The fraction $\sum_{u\in\mathscr{C}^+(v)} r_{vu} \le 1$ holds for all $v \in \mathscr{V}$ if $\mathscr{C}^+(v) \neq \emptyset$ because residents can choose other modes of transport such as walking or driving.
3. Effective population:
   We define the effective work-time population as $N^e_v(t) := \sum_{u\in\mathscr{N}^-(v)} r_{uv}N_u$, and the effective commuting population as $C^e_v(t) := \sum_{w\in\mathscr{C}^-(v)} r_{wv}N_v(t)$, respectively. The later definition holds by observing that commuters taking the same route back and forth so that $r_{vw} = r_{wv}$ for any $w \in \mathscr{C}^-(v)$. Let ρ define the transit matrix for r_{uv}, we can thus write the effective population as $N^e(t) = \rho_N^\intercal N(t)$ and $C^e(t) = \rho_C^\intercal N(t)$.

We call the expanded network a *commute network* $(\mathscr{V}, \mathscr{E})$. Using the *route* as the node representation in commute networks is because contagious diseases such as COVID-19 can spread via respiratory, aerosol, and contact transmission in vehicles. Experiments have shown that the infectious virus could be detected from surfaces for up to 24 hours or even three days (*17, 18*). This metapopulation model implies that travelers are exposed to the disease in a carriage carrying infectious passengers at different times. As a result, we only need to analyze the average daily traffic data to make day-to-day traffic control plans.

A common concern is that the traveling behavior may shift away from public transit systems because of the pandemic (*16*), and the government's disease control plans , such as reducing the public transit service time or alternative seating exacerbate this trend. It worth noticing that r_{vu} for each $v \in \mathscr{V}_{HW}$ and $u \in \mathscr{C}^+$ incorporates a route choice model. Since the common factors such as traveling time, trip purpose, and traffic congestion conditions still play a central role in these distributions, this work uses a fixed route choice models through the analysis. The demands for new empirical research regarding the change of the traveling behavior and calibrating the model with post-pandemic data is beyond the scope of this current work.

Spatial epidemic model

Spatial epidemic models are widely used to model the spread of infectious disease and quantify workable disease control strategies. Many infectious diseases have a long period from infection to onset of symptoms, which causes a significant challenge in addressing control strategies. The respiratory symptoms of COVID-19 appear in as few as two days or as long as 14 days after exposure (*18*). To capture this feature, we use a standard epidemic model that divide the population at each node into four groups, susceptible, exposed, infectious, and recovered as $S_v(t), E_v(t), I_v(t)$, and $R_v(t)$, respectively ; i.e., $N_v(t) = S_v(t) + E_v(t) + I_v(t) + R_v(t)$ for all $v \in \mathscr{V}_{HW}$. In each period, $Q_v(t) = \alpha(t) I_v(t)$ represents a ratio of the infectious population symptomatic and quarantined in the home node. The quarantined population is still contagious to the local population. The non-symptomatic individuals or individuals unaware of their health conditions, $(1-\alpha(t))I_v(t)$, continue to move in commute networks. The Spatial SEIR model on commute networks is presented in Figure 2.

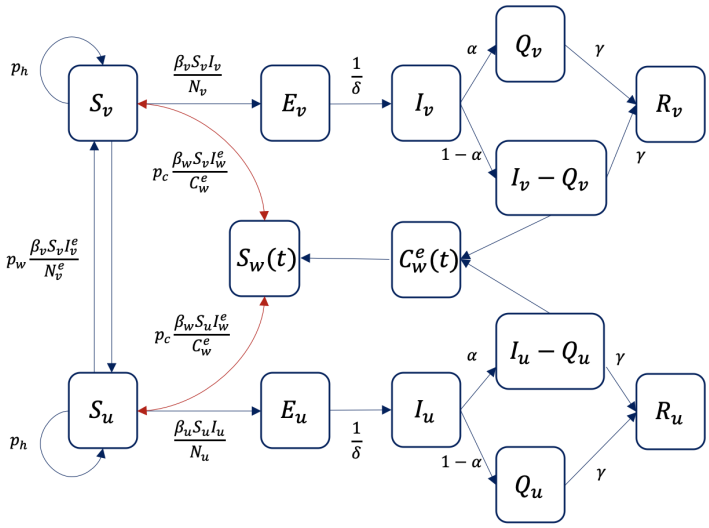

FIGURE 2: Spatial SEIR model on commute networks with $|\mathscr{V}_{HW}| = 2$ and $|\mathscr{V}_c| = 1$. In commute node w, C_w^e is the remaining flow-in commuter population through the transit route.

The dynamics of the susceptible population, who become exposed once having infectious contact with the infected population, is described as follows (*19*):

$$\begin{aligned}\frac{dS_v(t)}{dt} = &- p_H S_v(t)\left(\frac{(1-\alpha(t))\beta_v I_v(t)}{N_v}\right) - p_W S_v(t)\left(\sum_{u\in\mathscr{N}^+(v)} \frac{(1-\alpha(t))r_{vu}\beta_u[\rho_N I(t)]_u}{[\rho_N N]_u - \alpha(t)[\rho_N I(t)]_u}\right) \\ &- p_C S_v(t)\left(\sum_{w\in\mathscr{C}^+(v)} \frac{(1-\alpha(t))r_{vw}\beta_w[\rho_C I(t)]_w}{[\rho_C N]_w - \alpha(t)[\rho_C I(t)]_w}\right),\end{aligned} \tag{1}$$

where p_H, p_C and p_W represent the fraction of time during the day involving staying in the home region, commuting, and in the workplace, respectively. In each period, $(1-\alpha(t))$ ratio of the infected population is isolated from each node v. Note that we do not assume that each trip (u,v) is carried by public transit so the total $\sum_{v\in\mathscr{V}_{HW}}[\rho_C^\intercal N]_v \leq \sum_{v\in\mathscr{V}_{HW}} N_v$, and those use other modes such as driving bear no risk in commuting.

Following the notational conventions in epidemic models (*12, 20*), the epidemic model follows a Spatial SEIR model on commute networks:

$$\nabla_t \mathbf{S}_t = -p_H \mathbf{S}_t^\intercal \mathbf{I}_t^H - p_W \mathbf{S}_t^\intercal \mathbf{I}_t^W - p_C \mathbf{S}_t^\intercal \mathbf{I}_t^C, \tag{2}$$

$$\nabla_t \mathbf{E}_t = -\nabla_t \mathbf{S}_t - \frac{1}{\delta}\mathbf{E}_t, \tag{3}$$

$$\nabla_t \mathbf{I}_t = \frac{1}{\delta}\mathbf{E}_t - \gamma \mathbf{I}_t \tag{4}$$

$$\nabla_t \mathbf{R}_t = \gamma \mathbf{I}_t, \tag{5}$$

where δ is the latency period, and γ is the recovery rate. The spatial SEIR model guarantees that $dN_v/dt = 0$ for each $v \in \mathscr{V}_{HW}$ and $t \in \mathbb{R}^+$.These population vectors are given by:

$$\mathbf{S}_t = [S_v(t)]_{v\in\mathscr{V}}^\intercal, \qquad \begin{cases} \mathbf{I}_t^H = [\beta_v \frac{I_v(t)}{N_v}]_{v\in\mathscr{V}}^\intercal \\ \mathbf{I}_t^W = [\sum_{u\in\mathscr{N}^+(v)} r_{vu}\beta_u \frac{(1-\alpha(t))[\rho_N I(t)]_u}{[\rho_N N]_u - \alpha(t)[\rho_N I(t)]_u}]_{v\in\mathscr{V}}^\intercal \\ \mathbf{I}_t^C = [\sum_{w\in\mathscr{C}^+(v)} r_{vw}\beta_w \frac{(1-\alpha(t))[\rho_C I(t)]_w}{[\rho_C N]_w - \alpha(t)[\rho_C I(t)]_w}]_{v\in\mathscr{V}}^\intercal \end{cases}$$

Given the epidemic dynamics, we can obtain a critical measurement to guide disease control called the *basic reproduction number* R_0. It is the average number of secondary cases produced by one infected individual introduced into a completely susceptible population (*10*). Emerging infectious diseases such as COVID-19 can spread in a population if $R_0 > 1$. R_0 also determines what proportion of the population should be immunized or vaccinated to eradicate the infectious disease.

In the metapopulation setting, R_0 is defined as the dominant eigenvalue of the *next generation matrix* (NGM) $G_0 \in \mathbb{R}^{|\mathscr{V}_{HW}|\times|\mathscr{V}_{HW}|}$. Additionally, in the epidemiology literature there exists the concept of *effective reproductive number*, which we denote R_t, which measures the spread of the infection in a partially susceptible population. We extend this notion to the metapopulation model by computing the NGM and its dominant eigenvalue at time $t \neq 0$. The *effective next generation matrix*, G_t, is an approximate measurement of the disease transmission process for $t \in [0,T]$.

We can also obtain an expression for changes in R_t as a result of parameter changes in the model. For a fixed time t, let ζ and η be the eigenvectors associated with R_t in the eigenvector decomposition of G_t, i.e., $\zeta^\intercal G_t = R_t\zeta^\intercal, G_t\eta = R_t\eta$, and normalized such that $\zeta^\intercal\eta = 1$. If we vary the spatial SEIR model parameters by controlling the transit ridership through the planning horizon, we can evaluate the change of the reproduction number as:

$$\Delta R_t = \frac{\zeta^\intercal \Delta G_t \eta}{\zeta^\intercal \eta}. \tag{6}$$

Optimizing transit flows with disease reproduction constraints

Our decision is curbing the traffic flows on particular transit routes to balance the demand for commuting and disease spreading. For each $u \in \mathscr{V}_{HW}, w \in \mathscr{V}_C$, we let $x_{uw} \in [0,1]$ denote the proportion of subpopulation allowed to use this public transit route. Such a control can be realized either by reducing the frequency of service on a particular route or imposing new capacity regulation per ride. In the fixed flow control case, $\boldsymbol{x}$ is fixed at time $t = 0$; In the extended version, the policymaker adaptively changes the guidance for using public transit $\boldsymbol{x}(t)$ after observing that R_0 hits certain thresholds over the planning horizon $t \in [0,T]$.

Fixed flow control policy

Our decision $\boldsymbol{x} \in \mathbb{R}^{|\mathscr{V}_{HW}|\times|\mathscr{V}_C|}$ is the proportion of flows allow to use public transit on each route $(v,w), v \in \mathscr{V}_{HW}, w \in \mathscr{V}_C$. Our primary goal is to set an initial control plan to maximize the network throughput in public transit networks while protecting the public from the aggravation of infectious diseases. We can formulate the problem as follows:

$$\begin{aligned} &\text{maximize}_{\boldsymbol{x}} && \sum_{(v,w):v\in\mathscr{V}_{HW},w\in\mathscr{V}_C} x_{vw} r_{vw} N_v && (7)\\ &s.t. && \Delta R_0(\boldsymbol{x}) \le \kappa(R_0(1)-R_0(0)) \\ & && 0 \le x_{vw} \le 1, && \forall v \in \mathscr{V}_{HW}, \forall w \in \mathscr{V}_C. \end{aligned}$$

The right-hand side of the disease reproduction constraint in (7) means that the change of basic reproduction number due to opening public transit is within a tolerance $\kappa \in [0,1]$ from the worst case. The worst case is measured by R_0 with full reopening of public transit ($\boldsymbol{x} = 1$) and the best case is with no opening at all ($\boldsymbol{x} = 0$) (a more rigorous proof is given in Lemma 2). The main reasons for using this relative measure of the disease spreading, $R_0(1) - R_0(0)$, include:

1. The impact of controlling public transit flows not only affect the public transit users (direct exposed group), but also the resulting propagation to other populations in their home or work nodes.
2. The impact of public transit is sensitive to input data such as route choice estimation and epidemic model parameters. In contrast, the relative value of R_0 is a stable measure.
3. The constraint can be directly computed by (6).

Through the optimization, we assume that commuters choose alternative modes of transport (e.g., driving, walking, ride-hailing) if public transit is not available. This assumption is conservative for the estimation of disease spreading. Supposing that commuters disregard the travel plans if no alternative option is available, they are not exposed to the disease and our control policy is restricted for public safety.

We explain how to obtain the explicit expressions of constraints in what follows. The detailed derivations can be found in Appendix A.1. Assuming a constant quarantine ratio of α, the NGM at time t, $G_t(\boldsymbol{x})$, can be computed from the production of *transmission* and *transition* matrices. For each tuple of $u, v \in \mathscr{V}_{HW}$, we have:

$$\begin{aligned} [G_t(\boldsymbol{x})]_{vv} = \frac{1}{\gamma}\Big[& p_H \beta_v (1-\alpha)\frac{S_v(t)}{N_v} + p_W \sum_{u\in\mathscr{N}^+(v)} r_{vu}^2 \beta_u \frac{(1-\alpha)S_v(t)[\rho_N^\intercal N]_u}{([\rho_N^\intercal N]_u - \alpha[\rho_N^\intercal I(t)]_u)^2} + \\ & p_C \sum_{w\in\mathscr{C}^+(v)} x_{vw}^2 r_{vw}^2 \beta_w \frac{(1-\alpha)S_v(t)[\rho_C(x)^\intercal N]_w}{([\rho_C(x)^\intercal N]_w - \alpha[\rho_C(x)^\intercal I(t)]_w)^2}\Big], \end{aligned} \tag{8}$$

$$\begin{aligned} [G_t(\boldsymbol{x})]_{vu} = \frac{1}{\gamma}\Big[& p_W \sum_{w\in\mathscr{N}^+(u)\cap\mathscr{N}^+(v)} r_{uw} r_{vw} \beta_w \frac{(1-\alpha)S_v(t)[\rho_N^\intercal N]_w}{([\rho_N^\intercal N]_w - \alpha[\rho_N^\intercal I(t)]_w)^2} + \\ & p_C \sum_{w\in\mathscr{C}^+(u)\cap\mathscr{C}^+(v)} x_{uw} r_{uw} x_{vw} r_{vw} \beta_w \frac{(1-\alpha)S_v(t)[\rho_C(x)^\intercal N]_w}{([\rho_C(x)^\intercal N]_w - \alpha[\rho_C(x)^\intercal I(t)]_w)^2}\Big]. \end{aligned} \tag{9}$$

With fixed $\boldsymbol{x}$ over the planning horizon $t \in [0,T]$, the disease reproduction constraint in (7) is given by:

$$\zeta^\intercal(G_0(\boldsymbol{x})-G_0(0))\eta \le (R_0(1)-R_0(0))\zeta^\intercal\eta, \tag{10}$$

where $[G_0(\boldsymbol{x})-G_0(0)]_{vu} =$

$$\begin{cases} p_C \sum\limits_{w\in\mathscr{C}^+(v)} x_{vw}^2 r_{vw}^2 \beta_w (1-\alpha) S_v \dfrac{[\rho_C(x)^\intercal N]_w}{([\rho_C(x)^\intercal N]_w - \alpha[\rho_C(1)^\intercal I]_w)^2} & , v = u \\ p_C \sum\limits_{w\in\mathscr{C}^+(u)\cap\mathscr{C}^+(v)} x_{uw} r_{uw} x_{vw} r_{vw} \beta_w (1-\alpha) S_v \dfrac{[\rho_C(x)^\intercal N]_w}{([\rho_C(x)^\intercal N]_w - \alpha[\rho_C(x)^\intercal I]_w)^2} & , v \neq u. \end{cases}$$

Given controls $\boldsymbol{x}$, there exists an obvious disease-free equilibrium $S_v(0) = N_v$ and $I_v(0) = 0$ for all $v \in \mathscr{V}$ at $t = 0$. We can further simplify (10) as:

$$[G(\boldsymbol{x})-G(0)]_{vu} = \begin{cases} p_C(1-\alpha) N_v \sum\limits_{w\in\mathscr{C}^+(v)} \dfrac{x_{vw}^2 r_{vw}^2 \beta_w}{[\rho_C(x)^\intercal N]_w} & , v = u \\ p_C(1-\alpha) N_v \sum\limits_{w\in\mathscr{C}^+(u)\cap\mathscr{C}^+(v)} \dfrac{x_{uw} r_{uw} x_{vw} r_{vw} \beta_w}{[\rho_C(x)^\intercal N]_w} & , v \neq u. \end{cases} \tag{11}$$

Adaptive flow control policy

Corresponding to the disease control center's preparedness plans, the transportation authorities need to make sequential decisions during $[0,T]$ in the evolving situation. Since the basic reproduction number $R_t(x(t))$ represents the expected future infectious number after adopting the public transit control $x(t)$, we intend to design adaptive control policy around it. The optimal control policy is derived by solving the following extension of (7):

$$\begin{aligned} &\text{maximize} \sum_{\tau\in\boldsymbol{T}} \sum_{(v,w): v\in\mathscr{V}_{HW}, w\in\mathscr{V}_C} x_{vw}(\tau)\Delta\tau r_{vw} N_v && && (12)\\ s.t. \quad &\Delta R_\tau(\boldsymbol{x}(\tau)) \le \kappa_{R_\tau(0),R_\tau(1)}(\tau)\Big(R_\tau(1)-R_\tau(0)\Big), && \forall \tau \in \boldsymbol{T}, \\ &0 \le x_{vw} \le 1, && \forall v \in \mathscr{V}_{HW}, \forall w \in \mathscr{V}_C. \end{aligned}$$

Note that $\kappa_{R_t(0),R_t(1)}(t)$ is dependent on the values realized at period t as the public transit operator intends to lift the health measure constraints as the spreading of the disease slows down. As a result, the disease reproduction constraint is adaptive to the effect of traffic control policy up to time τ. Each control $\boldsymbol{x}(\tau)$ that persists for $\Delta\tau$ is added as a linear term in the objective. The policy-maker can set a series of thresholds for R_0 and the optimizer will return corresponding policies at periods $\boldsymbol{T} = \{0, \tau_1, \ldots, T\}$. Since the fixed flow control policy is a special case of the adaptive policy by setting $\boldsymbol{T} = \{0, T\}$ and $\boldsymbol{x}(\tau) = \boldsymbol{x}$, the adaptive policy is more effective than the fixed ones. Hence, we use the fixed control policy as a starting point for the adaptive control in Algorithm 1.

Solving adaptive control $t = [0,T]$ is more challenging due to the confounding simulation-and-optimization issue. Given policy $\boldsymbol{x}(\tau)$, simulating the spatial SEIR model is time-consuming and control-dependent. The workload grows exponentially when the list of thresholds increase. This urges to reduce the enumeration of controls by separating the compounds of simulation and optimization using the following procedure. We initialize Algorithm 1 with the fixed control policy. Then, in each backward step, we update the control policy after the current period and simulate the epidemic dynamics up to the current period. This procedure is valid because R_t is a long-term

measure for the contagious disease because of the prior controls. Given a sequence of controls along $\boldsymbol{T}$, the disease reproduction constraints have a knapsack structure and the objective function is linear in time horizon. The procedure is suboptimal because we do not enumerate all possible states of $\boldsymbol{S}_t$ and $\boldsymbol{I}_t$ and evaluate adaptive policies is costly.

Algorithm 1 Adaptive public transit flow control

Initial SEIR model $\boldsymbol{S}_0, \boldsymbol{E}_0, \boldsymbol{I}_0, \boldsymbol{R}_0$, population N, and network flow r over the commute network.
Solve fixed control problem $\hat{\boldsymbol{x}}$ and set the optimal control $\boldsymbol{x}(\tau) \leftarrow \hat{\boldsymbol{x}}$ for all $\tau \in \boldsymbol{T}$.
while $t \leq T$ **do**
  $\boldsymbol{x}(\tau) = \hat{\boldsymbol{x}}$ for $\tau < t$
  Let $t \leftarrow t + \Delta t$:
    · Forward step: Simulate spatial SEIR model and obtain $\boldsymbol{S}_t$ and $\boldsymbol{I}_t$.
    · Backward step: Solve the subproblems of optimization in (12) with $\boldsymbol{T} = [t, T]$ to obtain the optimal control $\boldsymbol{x}^*(\tau), \tau \geq t$ and optimal value $OPT(t)$. **Ensure:** $\Delta R_\tau(\boldsymbol{x}) \leq \kappa(\tau)(R_\tau(1) - R_\tau(0))$ for all $\tau \geq t$
  Update control by $\boldsymbol{x}(t) \leftarrow \boldsymbol{x}^*(t)$
  Update the objective value $OPT \leftarrow OPT(t)$
end while
return $\boldsymbol{x}(t)$ for $t \in \mathbf{T}$ amd the corresponding optimal value OPT.

In practice, we can integrate the data collection into the analysis as follows:

1. The observed infectious statistics can be used to calibrated the epidemic model $(\boldsymbol{S}_t, \boldsymbol{E}_t, \boldsymbol{I}_t, \boldsymbol{R}_t)$.
2. If interventions were not available in the early stage, we set $\boldsymbol{x} = 1$ for these periods and resolve the adaptive control problem in the middle of the disease outbreak.
3. Finally, we can work the optimal points of time $\boldsymbol{T}$ into the optimization as it is equivalent to enforcing new equality constrains on x over the planning horizon.

It worth noticing that the disease reproduction constraints in optimization (7) and (12) are non-convex and the dimension of $\boldsymbol{x} \in \mathbb{R}^{|\mathscr{V}_{HW}| \times |\mathscr{V}_C|}$ is large. In the next section, we specify the existence conditions for optimal control and general rules for the optimal fixed flow control policy.

GENERAL RULES FOR PUBLIC TRANSIT CONTROL POLICY

For ease of analysis, we study the fully connected commute networks where each home node is reachable from other work nodes, and each commute node in $\mathscr{V}_C$ connects to all nodes in $\mathscr{V}_{HW}$. This connectivity assumption does not lose generality because we can model inaccessible routes by enforcing the flow to be zero. The expanded network $(\mathscr{V}, \mathscr{E})$ is notwithstanding not fully connected because routes are not interconnected. The following lemma provides the existence conditions for optimal fixed control policy.

Lemma 1. *If the operator uses a global proportional control on public transit flow, i.e., x_{vw} is a constant for all $v \in \mathscr{V}_{HW}$ and $w \in \mathscr{V}_C$, the change of basic reproduction number is proportional to the control-free case.*

Proof. Let set $x_{vw} = \sigma$ for all $v \in \mathscr{V}_{HW}$ and $w \in \mathscr{V}_C$, which means that we allow a constant ratio of residents to use public transit on each route. We have $\rho_C(x) = \sigma \rho_C(1)$, and hence $\rho_C(x)^\intercal N = \sigma \rho_C(1)^\intercal N$ and $\frac{x_{vw}}{[\rho_C(x)^\intercal N]_w} = \frac{1}{[\rho_C(1)^\intercal N]_w}$. Note that $\frac{x_{vw}}{[\rho_C(x)^\intercal N]_w}$ appear in each entry of (11). This proves $\sigma[G(1) - G(0)] = G(\boldsymbol{x}) - G(0)$ and thus $\sigma[R_0(1) - R_0(0)] = R_0(\boldsymbol{x}) - R_0(0)$. □

Note that this lemma is true because we assume that people have access to alternative modes for commuting. Lemma 1 is an important building block as it means that, for any exogenous κ, we can simply set $\boldsymbol{x} = \kappa$ to satisfy the constraints hence the feasible set of the optimization is nonempty.

Definition 1. *A control policy $\boldsymbol{x}$ is more restrained than $\boldsymbol{x}'$ if:*

1. *$x_{vw} \le x'_{vw}$ for all $v \in \mathscr{V}_{HW}$ and $w \in \mathscr{V}_C$ and there exists edges such that $x_{vw} < x'_{vw}$.*
2. *Each pair of $x_{vw} > 0, x_{uw} > 0$ has dominating marginal effect on the controlled routes (v,w) and (u,w) with regard to the effective population, i.e., $\frac{x'_{vw}x'_{uv}}{x_{vw}x_{uw}} \ge \frac{[\rho_C(x')^\intercal N]_w}{[\rho_C(x)^\intercal N]_w}$.*

We then have the following lemma:

Lemma 2 (Monotonicity)**.** *If a public transit control policy $\boldsymbol{x}$ is more restrained than $\boldsymbol{x}'$, then $R_0(\boldsymbol{x}) < R_0(\boldsymbol{x}')$.*

Proof. Without loss of generality, we assume the NGM associated with $\boldsymbol{x}$ and $\boldsymbol{x}'$ both have linearly independent eigenvectors. NGM is nonnegative real-valued. We let the two NGM be $G := G_t(\boldsymbol{x})$ and $G' := G_t(\boldsymbol{x}')$. The difference $G' - G$ in each entry is:

$$\begin{cases} (1-\alpha)N_v p_C \sum_{w\in\mathscr{C}^+} \beta_w r_{vw}^2 \Big[\dfrac{x'^2_{vw}}{[\rho_C(x')^\intercal N]_w} - \dfrac{x^2_{vw}}{[\rho_C(x)^\intercal N]_w}\Big], & u = v \\ (1-\alpha)N_v p_C \sum_{w\in\mathscr{C}^+} \beta_w r_{vw} r_{uw} \Big[\dfrac{x'_{vw}x'_{uw}}{[\rho_C(x')^\intercal N]_w} - \dfrac{x_{vw}x_{uw}}{[\rho_C(x)^\intercal N]_w}\Big], & u \ne v. \end{cases}$$

Let $\boldsymbol{x}' = \boldsymbol{x} + \boldsymbol{\sigma}$. For an arbitrary $w \in \mathscr{V}_C$, we can plug $\boldsymbol{x}'$ into $G' - G$ so we can represent the NGMs as $G' = G + \boldsymbol{\sigma}' G$ with the perturbation $\sigma' G$ much smaller than G. We can observe that, if the conditions of restrained controls are satisfied, then each term above is nonnegative. Note that $\sigma' G \ge 0$ is a function of σ and x. According to the matrix perturbation theory (*21*), we have $\lambda'_i = \lambda_i + \eta_i^\intercal \sigma' G \eta$ for each eigenvalue λ_i. By definition, R_0 is the largest eigenvalue of NGM and we conclude that $R_0(\boldsymbol{x}') > R_0(\boldsymbol{x})$. □

Remark 1. *Lemma 2 indicates that reducing the traffic flow on a particular public transit route does not necessarily reduce the spreading of the infectious disease.*

Lemma 2 is not true if only condition 1 of restrained control holds. A counterexample is as follows. Instead of computing $\sigma' G$, we only need to show that, for any given $\boldsymbol{x}$ and arbitrary $u \in \mathscr{V}_{HW}, v \in \mathscr{V}_{HW}$, we have

$$[\sigma' G]_{vu} = \frac{(x_{vw} + \sigma_{vw})(x_{uw} + \sigma_{uw})}{[\rho_C(x)^\intercal N + \rho_C(\sigma)^\intercal N]_w} - \frac{x_{vw}x_{uw}}{[\rho_C(x)^\intercal N]_w}.$$

We can easily find $\sigma_{vw} > 0, \sigma_{uw} > 0$ such that $[\sigma' G]_{vu} < 0$ by having a third node v' with $N_{v'}\sigma_{v'w} \gg \sigma_{vw} + \sigma_{uw}$. Hence $R_0(\boldsymbol{x})$ increases with $\boldsymbol{x}$.

The optimization problem (7) is thus non-trivial because we cannot use gradient-based search method or decompose the problem by columns. The asymmetry between the home-and-work network and commute network motivates the derivation of the following general rules for obtaining upper-bounds on the public transit operations.

Theorem 1. *At the disease free equilibrium, with intervention $\boldsymbol{x}$, we have*

$$R_0(\boldsymbol{x}) \leq \frac{1-\alpha}{\gamma} \max_v \left[p_H \beta_v + p_W \sum_{w \in N^+(v)} r_{vw} \beta_w + p_C \sum_{w \in C^+(v)} x_{vw} r_{vw} \beta_w \right] \tag{13}$$

Proof. Since $R_0(\boldsymbol{x})$ is the spectral radius of $G(\boldsymbol{x})$, we have $R_0(\boldsymbol{x}) \leq \|G(\boldsymbol{x})\|$ for any induced matrix norm. Choosing the ℓ^1 norm, we have

$$R_0(\boldsymbol{x}) \leq \|G_0\|_{\ell^1} = \max_v \sum_{u=1}^{n} [G_0(\boldsymbol{x})]_{uv}.$$

Computing the sum of column v of $G_0(\boldsymbol{x})$, we get

$$\begin{aligned}
\sum_{u=1}^{n} [G_0(\boldsymbol{x})]_{uv} &= \frac{p_H(1-\alpha)}{\gamma} \beta_v + \frac{p_W(1-\alpha)}{\gamma} \sum_{u=1}^{n} \sum_{w=1}^{n} r_{uw} r_{vw} \beta_w \frac{N_u}{[\rho_N^\intercal N]_w} \\
&\quad + \frac{p_C(1-\alpha)}{\gamma} \sum_{u=1}^{n} \sum_{w=1}^{m} x_{uw} r_{uw} x_{vw} r_{vw} \beta_w \frac{N_u}{[\rho_C(x)^\intercal N]_w} \\
&= \frac{p_H(1-\alpha)}{\gamma} \beta_v + \frac{p_W(1-\alpha)}{\gamma} \sum_{w=1}^{n} r_{vw} \beta_w + \frac{p_C(1-\alpha)}{\gamma} \sum_{w=1}^{m} x_{vw} r_{vw} \beta_w.
\end{aligned}$$

Taking the maximum over v gives the desired expression. □

Remark 2. *This bound can be further simplified to*

$$R_0(\boldsymbol{x}) \leq \frac{(1-\alpha) \max_v \beta_v}{\gamma} \left(p_H + p_W + p_C \max_{v,w} x_{vw} \right) \tag{14}$$

which makes clear the relationship to R_0 in the single population model, which would be given by $\frac{(1-\alpha)\beta}{\gamma}$.

Theorem 2. *Assume we have a policy $\boldsymbol{x}$ that is more restrained than having no intervention. Then at the disease free equilibrium $\Delta R_0(\boldsymbol{x}) = R_0(1) - R_0(\boldsymbol{x})$ satisfies*

$$0 \leq \Delta R_0(\boldsymbol{x}) \leq \|\xi\|_{\ell^1} \|\eta\|_{\ell^1} \max_v \sum_{w \in C^+(v)} r_{vw} \beta_w (1 - x_{vw}), \tag{15}$$

where ξ and η are the left and right eigenvectors of $G_0(1)$ normalized such that $\xi^\intercal \eta = 1$.

Proof. The inequality $0 \leq \Delta R_0(\boldsymbol{x})$ follows from Lemma 2. Taking norms on both sides of the sensitivity analysis equation we get

$$|\Delta R_0(\boldsymbol{x})| \leq \|\xi\| \|\eta\| \|\Delta G_0(\boldsymbol{x})\|$$

for any induced matrix norm. Again choosing ℓ^1, we have

$$
\begin{aligned}
\|\Delta G_0(\boldsymbol{x})\|_{\ell^1} &= \max_v \sum_{u=1}^{n} [\Delta G_0(x)]_{uv} \\
&= \frac{p_C(1-\alpha)}{\gamma} \max_v \sum_{w=1}^{m} r_{vw}\beta_w \left(\frac{\sum_{u=1}^{n} r_{uw}N_u}{[\rho_C(1)^\intercal N]_w} - \frac{x_{vw}\sum_{u=1}^{n} x_{uw}r_{uw}N_u}{[\rho_C(x)^\intercal N]_w} \right) \\
&= \frac{p_C(1-\alpha)}{\gamma} \max_v \sum_{w=1}^{m} r_{vw}\beta_w (1-x_{vw})
\end{aligned}
$$

which gives the result. Note that each term in the sum is positive because of the definition of restrained policies. □

Proposition 1. *To maximize the upper bound (maximize the potential impact on R_0) we should choose a policy x such that*

$$
\boldsymbol{x} = \arg\max_{\boldsymbol{x}} \left[\max_v \sum_{w=1}^{m} r_{vw}\beta_w (1-x_{vw}) \right] \tag{16}
$$

Remark 3. *These bounds can be extended to the case of $G_t(\boldsymbol{x})$, and other bounds can be obtained by considering other vector norms.*

Proposition 2. *The basic reproduction number $R_t(\boldsymbol{x}) < 1$ for any $t \in [0,T]$ if and only if*

$$
\lim_{k\to\infty} G_t(\boldsymbol{x})^k = 0. \tag{17}
$$

Proposition 2 holds due to the convergence of the power series of the NGM as R_0 is the spectral radius of NGM for any control $\boldsymbol{x}$. This condition has valuable practical meaning because $R_0 < 1$ is a central indicator that the infection cannot spread in a population.

In summary, solving for optimal flow control policies in (7) or (12) is computational challenging because of the nonlinear disease reproduction constraints. We can leverage general observations drawn above to improve computational efficiency. Besides, these observations also have important policy implications regarding transit-relate disease control plans.

NUMERICAL RESULTS AND CASE STUDY

We validate the general rules for public transit control policies in §5.1 the test the impact of input data in §5.2. In §5.3, we present the improvement of adaptive control policy. To solve a case study of NYC's subway system in §5.4, we investigate the impact of network complexity as a critical building block for large-scale networks.

Calibrating metapopulation and epidemic models

We combine multiple sources of data to gauge the metapopulation model and the epidemic model. Table 1 summarizes the epidemic model's parameters from existing COVID-19 literature and the calibrated traffic flow data used in the rest of the numerical experiments. We study the NYC case study because it has one of the largest public transit systems in the world. About 39% of the population in NYC use public transit for commuting, more than that of driving private cars (27%) (*22*). NYC was also one of the cities with the most COVID-19 cases in the first half of 2020.

Although the ridership of the subway witnessed a significant drop (*16*) amid the early stage of the pandemic, we hope to propose a safe and effective management policy during the recovery time.

Parameter	Epidemic model			
	Average contagion rate $\bar{\beta}$	Length of infectious period $1/\gamma$	Length of latent period δ	Quarantine ratio α
Value	0.422 (*23*)	6.5 days (*24*)	5.1 days (*25*)	0.15 (*26*)
Parameter	Public transit network			
	Origin-destination daily flow	Subway ridership in pandemic	Transit network transfer connectivity	
Source	Regional MTA (*27*)	Wang et al. (*16*)	Regional MTA (*27*)	
Parameter	Spatial SEIR weights (*28*)			Constraint κ
	Hours active at home	Hours in work	Commute time	
Value	8 hr	8 hr	1 hr	0.5

TABLE 1: Parameters and data sources for NYC case study

In addition, we can obtain the local contagion rate β_v by:

$$\beta_v = \bar{\beta} \cdot \frac{d_v}{\bar{d}}, \forall v \in \mathcal{V}, \tag{18}$$

where d_v is the population density in region v and $\bar{d}$ is the average population density.

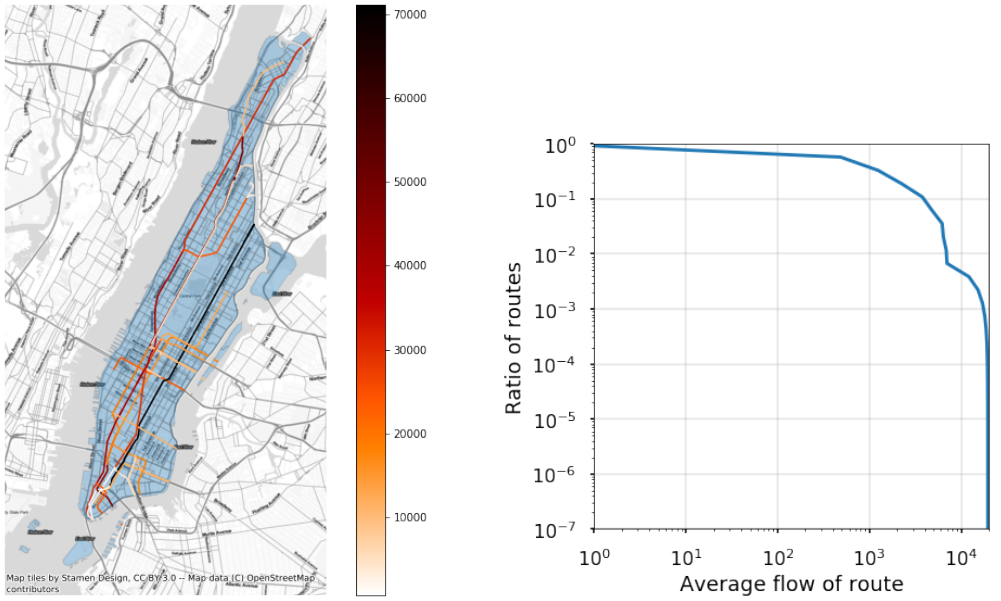

(a) Manhattan subway system's average daily commuting flow estimation

(b) Commute networks' route flow distribution

FIGURE 3: Case study: controlling public transit (subway) in Manhattan, NYC dueing the outbreak of COVID-19 in 2020.

Given the population N_v for $v \in \mathcal{V}_{HW}$ and daily commuting flows on the home-to-work network, we need to determine the probability of choosing each route r_{vw} for each $v \in \mathcal{V}_{HW}$ and

$w \in \mathscr{V}_C$. Assuming that each potential commuter following a multinomial logit model (MNL) with a single explanatory variable – the walking distance to the route:

$$r_{vw} = P(y = w|d_w) = \frac{\exp(\varepsilon d_w)}{\sum_{w' \in \mathscr{V}_C} \exp(\varepsilon d_{w'})}, \tag{19}$$

where y is the dependent variable for route choice, d_w is the Manhattan distance to the subway line, and ε is a constant depending on commuters' heterogeneity. Also, we assume that commuters use the same route from home to work and back (*10, 20*). Each route's flow $w \in \mathscr{V}_C$ is $\sum_{v \in \mathscr{V}_{HW}} r_{vw} N_v$ as shown in Figure 3a. This route choice estimation is arguably inaccurate. We use two strategies to enhance the accuracy of the route choice model. First, we reweigh the routing probabilities by the MTA subway ridership data (*27*) because trips other than commuting are also important components in the infectious contact in public transit. Second, §5.2 shows that optimal control policies are insensitive to these estimation errors.

Spatially-specific controls on public transit are necessary only if the underlying network's features such as density or degree have a heavy-tailed distribution (*10*). The distributional assumption is verified as the estimated distributions of the subway flow $\sum_{v \in \mathscr{V}_{HW}} r_{vw} N_v$ in Manhattan, NYC is obviously heavy-tailed in Figure 3b.

Aggregating commute networks and sensitivity analysis

We conduct three types of sensitivity analysis to understand the errors caused by model reductions and the input data inaccuracy.

- **Test on route choice:** A sensitivity analysis of the route choice model.
- **Test on commute network characteristics:** A sensitivity analysis of network properties such as network degrees.
- **Test on epidemic model:** A sensitivity analysis of the epidemic model's parameters.

Test on route choice: The first sensitivity analysis is conducted on a well-designed commute network having fixed origin-destination flows (sorted from large to small in Figure 13 in A.2). Residents follow a random route choice model with a uniform distribution. Unlike the distance-based choice model in the case study, we randomize the route choice because the actual route choice is difficult to estimate without trajectory data and may differ before and after the outbreak of the infectious disease. Our goal is to evaluate the variations of both objective and the reproduction rate of the emerging disease when people's route choice shifts from their normal routine.

We simulate $1,000$ experiments and compute the optimal controls for public transit flow repeatedly from (7). The upper bound for the total transit throughput of about 85 depends on the sampled choice model. Note that, if there is no intervention in commute networks, i.e., $\boldsymbol{x} = 1$, the disease spreads with $R_0 = 1.75$; if the public transit is shut down, the disease is under control with $R_0 = 1.39$. Hence, the implementation of public transit flow controls is critical for public safety. We draw the following observations from the experiments:

1. The optimal control $\boldsymbol{x}$ is small for nodes with the large outflows and vice versa.
2. The objective and optimal controls $\boldsymbol{x}$ is relatively sensitive to the uncertain route choice (Figure 4a) because r are linear coefficients in the objective.
3. The disease reproduction constraint is sensitive to the route choice model (Figure 4b).

We conclude that the accurate estimation for the route choice model is critical for the optimality of control plans. Hence, travel behaviors during the on-peak and post-pandemic time need further investigation.

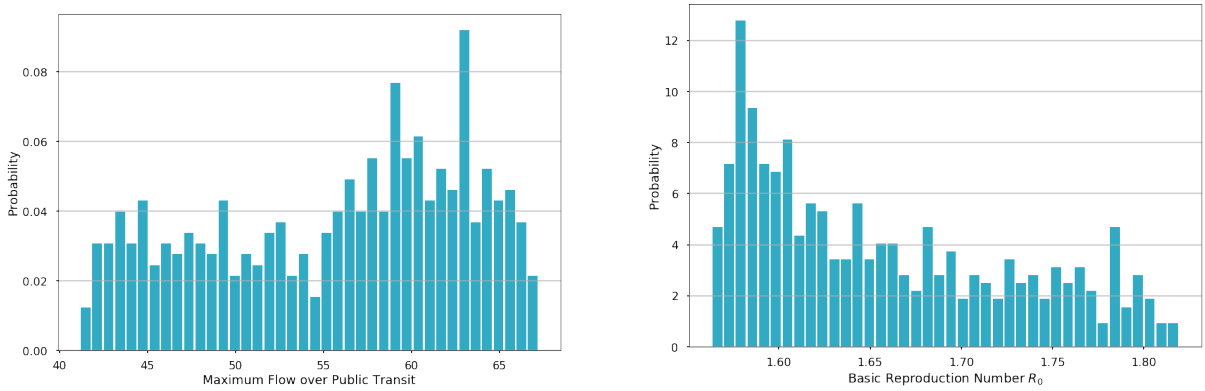

(a) Effect on maximum flow

(b) Effect on basic reproduction number

FIGURE 4: Sensitivity of fixed optimal transit flow controls with regard to the random route choice

Test on commute network characteristics: We solve the fixed transit flow controls by non-convex programming in (7) with increasing number of nodes. The computation time grow sub-exponentially as the size of the problem ($|\boldsymbol{x}| = |\mathscr{V}_{HW} \times \mathscr{V}_C|$) increases (Figure 5).

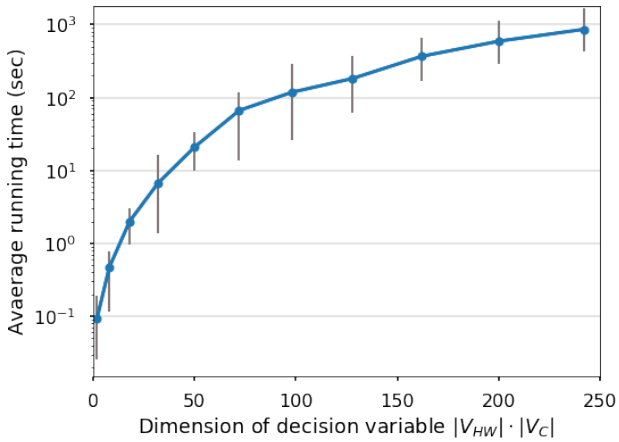

FIGURE 5: Optimization (7)'s running time grows with the network size

Thus, the large-scale problem quickly becomes unsolvable mainly due to the nonlinearity of the disease reproduction constraint. Reducing network size is necessary for the NYC case study containing 288 census tract nodes and 277 routes. Extrapolating the running time in Figure 5, computing the exact solution of the NYC network ($|\boldsymbol{x}| \approx 80,000$) by standard nonlinear programming methods is obviously impractical. In this case, the trust-region method is expected to take $10^{15} - 10^{23}$ seconds to solve to optimally.

To handle such a large-scale network analysis, we can cluster nodes in $\mathscr{V}_{HW}$ with similar demographical information and aggregate the inter-node commuting flows. The question of optimality loss due to this node-aggregation procedure naturally arises. In the following experiment, we keep the constant total expected population $\|N\|_1 = 100$ when dividing the area of interest to finer and finer grids. Consequently, the degree of the fully-connected commute networks (i.e., the

number of connections it has to other nodes) increases. For example, when dividing the area evenly into two nodes, the maximum degree of the network is 3, and so on.

When the maximum degree of the commute network increases, the objective value of (7) is stable, but the basic reproduction number increases significantly. When the degree increases, the impact of critical nodes is strengthened, so the basic reproduction number at optimality increases accordingly. This is another reason not to use the absolute value of R_0 when scaling the networks for computational efficiency. However, as (7) and (12) use a relative reduction in basic reproduction number, the results are unaffected to the scaling of the commute networks except the control policies become less specific.

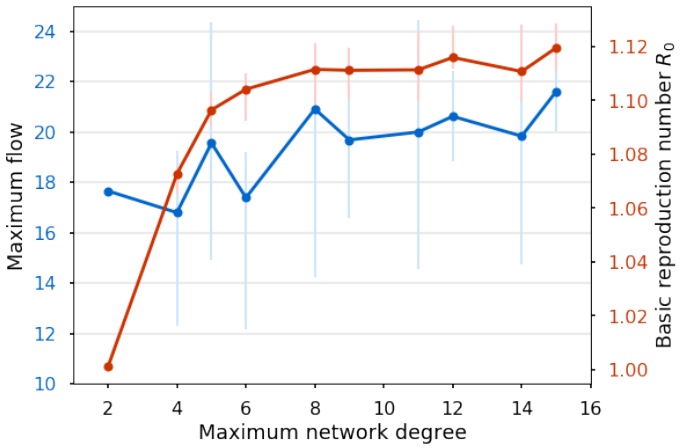

FIGURE 6: Sensitivity of the optimal control and the basic reproduction number regarding the commute network's degree

Test on epidemic model: The accuracy of the epidemic model is highly dependent on the estimated parameters in Table 1. However, these parameters, especially the contagion rate from the susceptible population S to the infected population I, are affected by the anti-contagion policies (*29*) and social responsiveness(*30*). For example, the transmission rate β reported in literature varies from 0.17 to 0.8 (*16, 23–25*) because of the social distancing effect. We test the sensitivity of objective function in (7) and basic reproduction number with varying parameters from literature. The sensitivity test results are shown in Figure 7.

We draw the following observations:

1. As the average contagion rate $\bar{\beta}$ increases due to lack of prevention strategies such as social-distancing, the maximum public transit flow decreases to control the transmission. On the other hand, the basic reproduction number increases substantially.
2. As the quarantine ratio α increases, for example, the testing rate increases so more infected population is identified, the maximum public transit flow stays approximately the same while the basic reproduction number decreases substantially.
3. As the length of the infection period increases due to the deterioration of healthcare quality, the maximum public transit flow decreases because of the significant increase in the basic reproduction number.
4. The latent period's length has a negligible impact on the optimal control policy or the disease spreading speed.

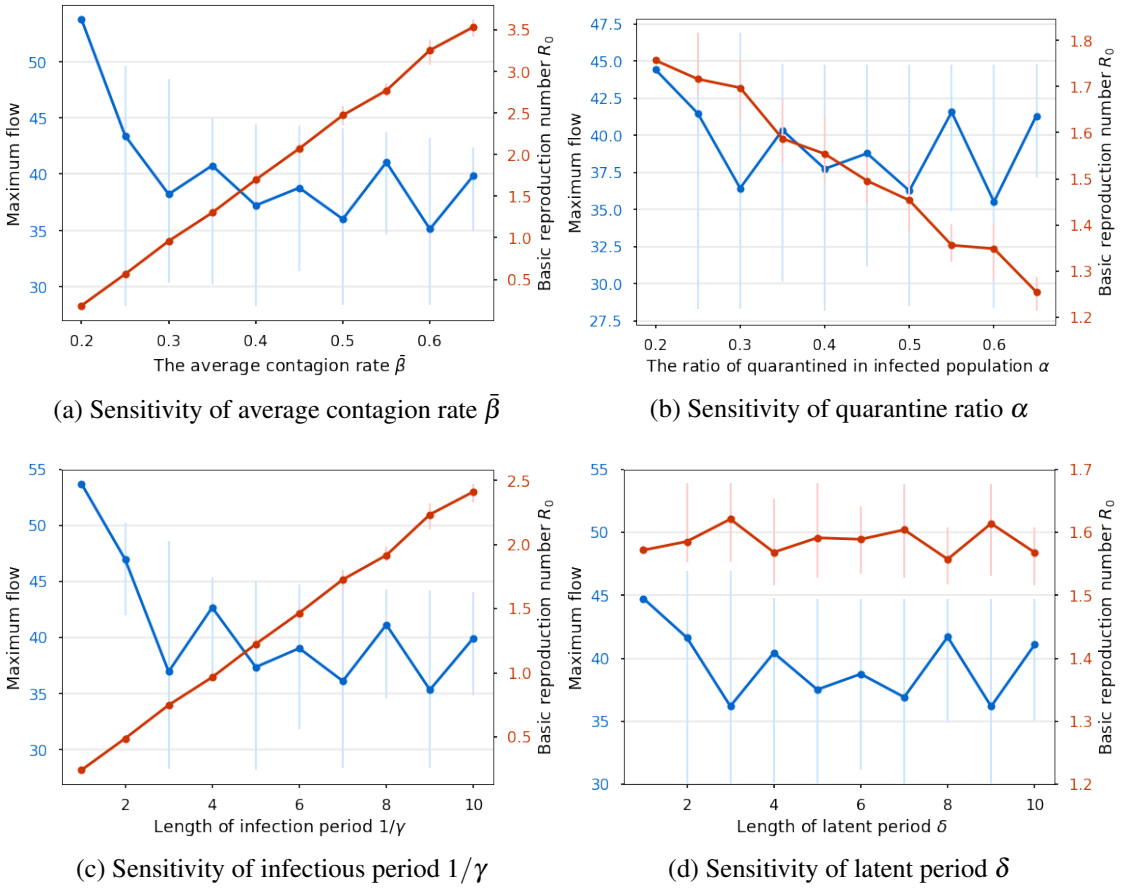

(a) Sensitivity of average contagion rate $\bar{\beta}$

(b) Sensitivity of quarantine ratio α

(c) Sensitivity of infectious period $1/\gamma$

(d) Sensitivity of latent period δ

FIGURE 7: Sensitivity analysis of epidemic model parameters

Social-distancing strategy on public transit: If public transit operators enforce stricter social-distancing policies in vehicle, β_w is reduced for all $w \in \mathcal{V}_C$. Such a policy can assist the control of the disease as shown in Figure 8. We vary the ratio of $\beta_w/\bar{\beta}$ and the basic disease reproduction number is reduced. As we are using a relative disease reproduction constraint, the objective function is not much affected. To this end, social-distancing in public transit helps the public health measures and do not affect the maximal throughput in commute networks.

Health-and-economics trade-off: The health-and-economics trade-off reflects by the value of κ in the disease reproduction constraint. When κ increases from 0 to 1, the system puts more weight on efficiency and less weight on safety. As shown in Figure 9, when the total throughput in commute networks increases significantly. Note that the variation of the objective is large when κ is between $0.2-0.6$. In the case study of NYC, the same trade-off is presented in the subway operational plans.

Numerical results for adaptive flow control

We demonstrate the insights obtained by solving a two-stage adaptive policies in the same network presented above. The computation of the dynamic policy in Algorithm 1 allows to iteratively simulate the state $\boldsymbol{S}_t$ and $\boldsymbol{I}_t$ are dependent on $\boldsymbol{x}(\tau), \tau < t$. On the other hand, the disease reproduction constraints need to satisfied for all $\tau \in \boldsymbol{T}$.

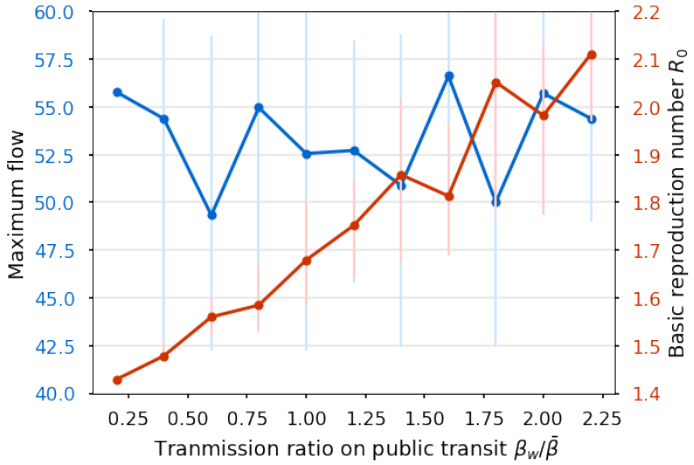

FIGURE 8: Effect of social-distancing policy on public transit

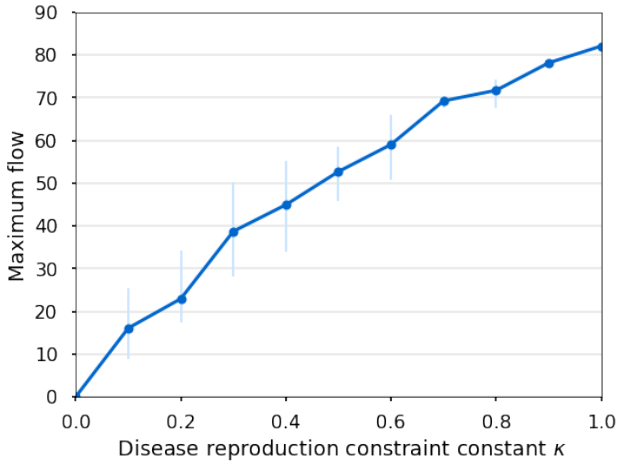

FIGURE 9: Health-and-economics trade-off

$\kappa(\tau)$ is a sequence of endogenous variables that mitigates the health-and-economics trade-off due to the evolving pandemic. As the constraint $\kappa_{R_0(0),R_0(1)}(t)$ is dependent on the realized basic reproduction number at time t, the optimization automatically adjusts more weights on economics than health concerns as the severeness of the disease relieves. Suppose that we make an initial flow control policy at $t = 0$ and allow to adjust the policy at $t' \in [0,T]$ when $R_0(1)$ hits a preset threshold. To demonstrate the strictness of the health measures after the basic reproduction number $R_0(t')$, we fix $\kappa(0) = 0.5$ and sampling points with $\kappa(t') = R_0(0,t')/R_0(0,0)$. As $R_0(0,t')/R_0(0,0)$ increases, the second state decision is made earlier. Note that $\kappa(t') \approx 1.0$ is equivalent to relaxing the disease reproduction constraint.

In Figure 10, the maximum flow over the public transit network increases as the health measures are more severe at the early stage. In other words, setting a large threshold for a sequential decision increase the total throughput; thus, quick responsiveness is valuable for social benefit. On each route and location, we also observe the inhomogeneous level of relieved flow in Figure 14 in Appendix A.2 when κ decreases or increases because (12) automatically and effectively releases

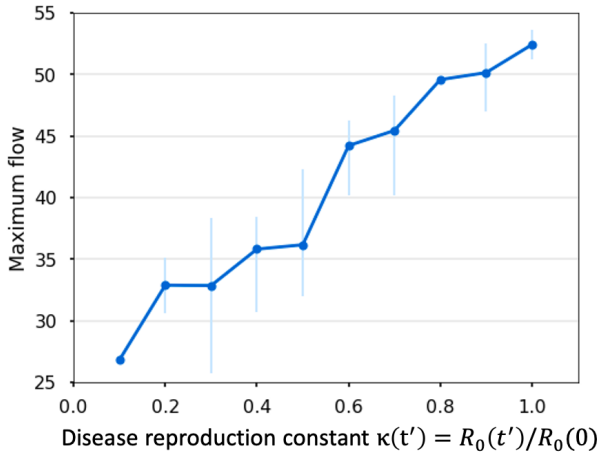

FIGURE 10: The optimal control when the health measures are relaxed over time

the restrictions on public transit traffic after observing the changes of the disease dynamics.

Trade-offs in NYC's reopening decisions

Obtaining the control policy directly for complex urban infrastructure networks is computationally challenging. Owing to the small optimality gap shown in the sensitivity test, this procedure does not influence the results' generality. Considering commuters' transfers, the NYC subway system contains 277 *combinations of subway lines*, hence $|\mathcal{V}_C| = 277$ in the following analysis (transfers between subway lines can refer to Appendix A.2). The census tracts in Manhattan, NYC are combined to 15 nodes (labeled 0-14 in Figure 11a) by spatial clustering.

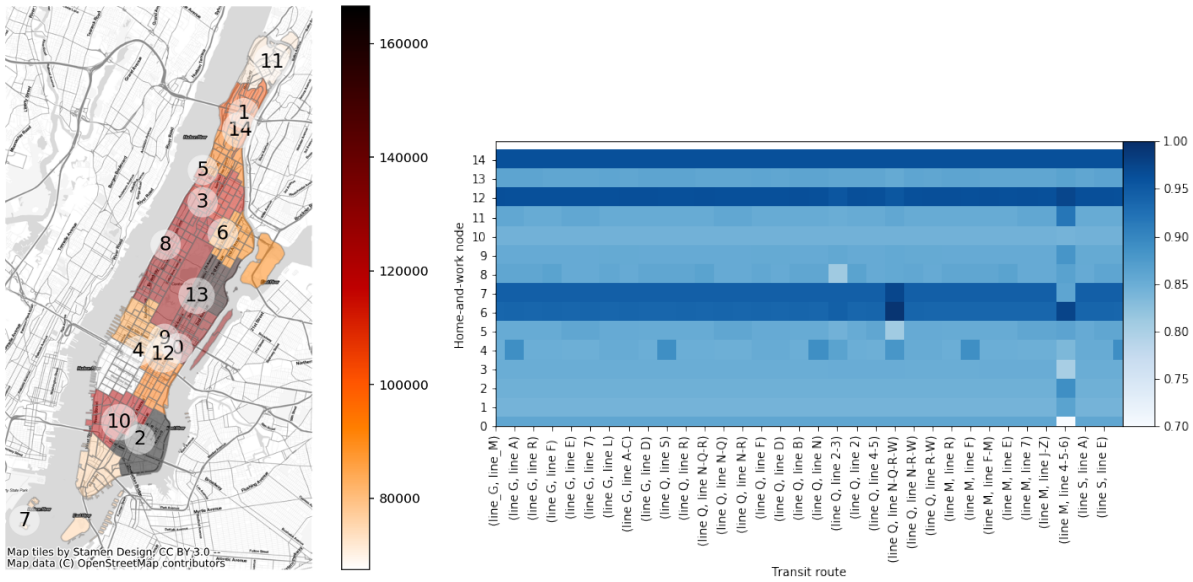

(a) Susceptible population N at $t = 0$ in aggregate home-and-work network $\mathcal{V}_{HW}$

(b) Optimal public transit control $\mathbf{x}$

FIGURE 11: Optimal public transit control policy in NYC case study

We focus on the fixed traffic flow control policy in this case study. With no intervention on public transit (i.e., $\boldsymbol{x} = 1$), the basic reproduction number is $R_0(1) = 1.794$; with the total closure of public transit, $R_0(0) = 1.670$. The optimal control policy shown in Figure 11b obtains 88% (original network flow is 1.62 million) while reducing the gap of the basic reproduction rate at $R_0 = 1.703$.

Although the difference in basic reproduction number seems small, mainly due to the short time spent in transit per day p_C, its effect on transmitting the infectious disease is significant. As we can see the dynamics in Figure 12, the difference between the optimal control and no-control scenarios can reach $50,000$ for the susceptible population, and $30,000$ for the infected population in Manhattan borough within $T = 100$ days. These results emphasize the need for controlling the disease transmission on the target region or public transit line during the reopening time, especially with the anticipated second-wave (*31*).

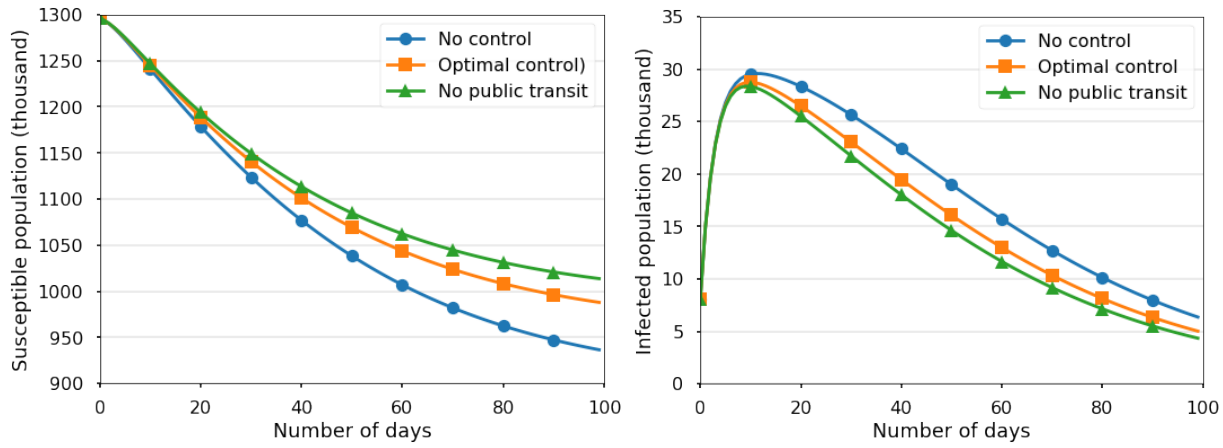

(a) Susceptible population

(b) Infected population

FIGURE 12: Dynamics of COVID-19 under different public transit control policies

Regarding the route-level controls in Figure 12b, we make two additional remarks.

Remark 4 (Critical nodes in commute networks)**.** *In fully connected commute networks, the disease reproduction constraint is most sensitive to controls implemented on areas with largest outflow.*

Remark 5 (Route-based control)**.** *Limiting flow on a high-density route does not necessary control the spreading speed of the disease most effectively.*

Note that Remark 4 is consistent with the sensitivity analysis in (*10*). The R_0-centrality measure is defined as $-\frac{\partial \lambda_0(G)}{\partial N_v}$, which is equivalent to the sensitivity analysis on x_{vw} in the current work.

Finally, the results provide several interesting policy implications that can also be generalized to other cities' disease control plans:

1. The numerical results in NYC confirm the general rules derived in §4. For example, the optimal subway control policy is almost uniform on each row (corresponding to a home-and-work node) in Figure 11a. The most populated outflow node is curtailed the most.

2. Shutting down public transit, as passengers may choose alternative modes, brings marginal benefit comparing to the targeted traffic control policy in this work (Figure 12).

CONCLUSION

This work proposes a disease reproduction constrained mathematical programming to resolve the health-and-economics trade-offs in responsiveness plans for pandemics. An optimization-based analysis simultaneously accommodates the inevitable travel demand amid the pandemic period and reopening the economy and meanwhile follows the strict safety measures for the infectious disease. By maximizing the transit flow constrained by the epidemic prevention measures requirement, public transit continues to serve as a protected, low-emission, and low-cost option in urban transportation.

Note that the node-target public transit control policy has a potential equity issue in extreme cases. In the case study, we restrict most lines between 40% and 90% due to the demographical similarity in Manhattan, NYC. We can avoid this issue by either proposing new lower bounds for controls $\boldsymbol{x}$ or reformulating the objective to a max-min problem. Another promising research avenue is to investigate more realistic models, such as stochastic epidemic models and heterogeneous traveling behavior.

ACKNOWLEDGEMENTS

The authors would like to thank Juan Carlos Martinez Mori and Doreen Gui at Cornell University, Benedetto Piccoli at Rutgers University, and William Barbour and Dan Work at Vanderbilt University for their assistance and advise.

REFERENCES

1. van Dorn, A., R. E. Cooney, and M. L. Sabin, COVID-19 exacerbating inequalities in the US. *The Lancet*, Vol. 395, No. 10232, 2020, pp. 1243–1244.
2. Cohen, J. and K. Kupferschmidt, Countries test tactics in'war'against COVID-19. *Science*, Vol. 367, No. 6484, 2020, p. 1287.
3. Lewnard, J. A. and N. C. Lo, Scientific and ethical basis for social-distancing interventions against COVID-19. *The Lancet. Infectious diseases*, 2020.
4. Amekudzi-Kennedy, A., S. Labi, B. Woodall, M. Chester, and P. Singh, Reflections on Pandemics, Civil Infrastructure and Sustainable Development: Five Lessons from COVID-19 through the Lens of Transportation, 2020.
5. DeWeese, J., L. Hawa, H. Demyk, Z. Davey, A. Belikow, and A. El-geneidy, A Tale of 40 Cities: A Preliminary Analysis of Equity Impacts of COVID-19 Service Adjustments across North America. *Transport Findings*, 2020.
6. Feng, S., C. Shen, N. Xia, W. Song, M. Fan, and B. J. Cowling, Rational use of face masks in the COVID-19 pandemic. *The Lancet Respiratory Medicine*, Vol. 8, No. 5, 2020, pp. 434–436.
7. Keeling, M. J., L. Danon, M. C. Vernon, and T. A. House, Individual identity and movement networks for disease metapopulations. *Proceedings of the National Academy of Sciences*, Vol. 107, No. 19, 2010, pp. 8866–8870.
8. Balcan, D. and A. Vespignani, Phase transitions in contagion processes mediated by recurrent mobility patterns. *Nature physics*, Vol. 7, No. 7, 2011, pp. 581–586.
9. Bichara, D. and A. Iggidr, Multi-patch and multi-group epidemic models: a new framework. *Journal of mathematical biology*, Vol. 77, No. 1, 2018, pp. 107–134.
10. Yashima, K. and A. Sasaki, Spotting Epidemic Keystones by R0 Sensitivity Analysis: High-Risk Stations in the Tokyo Metropolitan Area. *PloS one*, Vol. 11, No. 9, 2016, p. e0162406.
11. Zhou, Y., J. Wang, and H. Yang, Resilience of transportation systems: concepts and comprehensive review. *IEEE Transactions on Intelligent Transportation Systems*, 2019.
12. Mo, B., K. Feng, Y. Shen, C. Tam, D. Li, Y. Yin, and J. Zhao, Modeling Epidemic Spreading through Public Transit using Time-Varying Encounter Network. *arXiv preprint arXiv:2004.04602*, 2020.
13. Qian, X., L. Sun, and S. V. Ukkusuri, Scaling of contact networks for epidemic spreading in urban transit systems. *arXiv preprint arXiv:2002.03564*, 2020.
14. Chang, S. Y., E. Pierson, P. W. Koh, J. Gerardin, B. Redbird, D. Grusky, and J. Leskovec, Mobility network modeling explains higher SARS-CoV-2 infection rates among disadvantaged groups and informs reopening strategies. *medRxiv*, 2020.
15. Lee, S. G. and M. Hickman, Trip purpose inference using automated fare collection data. *Public Transport*, Vol. 6, No. 1-2, 2014, pp. 1–20.
16. Wang, D., B. Y. He, J. Gao, J. Y. Chow, K. Ozbay, and S. Iyer, Impact of COVID-19 behavioral inertia on reopening strategies for New York City transit. *arXiv preprint arXiv:2006.13368*, 2020.
17. Van Doremalen, N., T. Bushmaker, D. H. Morris, M. G. Holbrook, A. Gamble, B. N. Williamson, A. Tamin, J. L. Harcourt, N. J. Thornburg, S. I. Gerber, et al., Aerosol and surface stability of SARS-CoV-2 as compared with SARS-CoV-1. *New England Journal of Medicine*, Vol. 382, No. 16, 2020, pp. 1564–1567.

18. Chin, A. W., J. T. Chu, M. R. Perera, K. P. Hui, H.-L. Yen, M. C. Chan, M. Peiris, and L. L. Poon, Stability of SARS-CoV-2 in different environmental conditions. *The Lancet Microbe*, Vol. 1, No. 1, 2020, p. e10.
19. Mori, J. C. M., W. Barbour, D. Gui, B. Piccoli, D. Work, and S. Samaranayake, *A Multi-Region SEIR Model with Mobility*. `https://seir.cee.cornell.edu`, 2020.
20. Qian, X. and S. V. Ukkusuri, Modeling the spread of infectious disease in urban areas with travel contagion. *arXiv preprint arXiv:2005.04583*, 2020.
21. Bhatia, R., *Perturbation bounds for matrix eigenvalues*. SIAM, 2007.
22. Tajalli, M. and A. Hajbabaie, On the relationships between commuting mode choice and public health. *Journal of Transport & Health*, Vol. 4, 2017, pp. 267–277.
23. Prem, K., Y. Liu, T. W. Russell, A. J. Kucharski, R. M. Eggo, N. Davies, S. Flasche, S. Clifford, C. A. Pearson, J. D. Munday, et al., The effect of control strategies to reduce social mixing on outcomes of the COVID-19 epidemic in Wuhan, China: a modelling study. *The Lancet Public Health*, 2020.
24. Yang, Z., Z. Zeng, K. Wang, S.-S. Wong, W. Liang, M. Zanin, P. Liu, X. Cao, Z. Gao, Z. Mai, et al., Modified SEIR and AI prediction of the epidemics trend of COVID-19 in China under public health interventions. *Journal of Thoracic Disease*, Vol. 12, No. 3, 2020, p. 165.
25. Lauer, S. A., K. H. Grantz, Q. Bi, F. K. Jones, Q. Zheng, H. R. Meredith, A. S. Azman, N. G. Reich, and J. Lessler, The incubation period of coronavirus disease 2019 (COVID-19) from publicly reported confirmed cases: estimation and application. *Annals of internal medicine*, Vol. 172, No. 9, 2020, pp. 577–582.
26. Nishiura, H., T. Kobayashi, T. Miyama, A. Suzuki, S.-m. Jung, K. Hayashi, R. Kinoshita, Y. Yang, B. Yuan, A. R. Akhmetzhanov, et al., Estimation of the asymptomatic ratio of novel coronavirus infections (COVID-19). *International journal of infectious diseases*, Vol. 94, 2020, p. 154.
27. NYC, M., *The Metropolitan Transportation Authority of New York City*. `http://web.mta.info/mta/planning/data.html`, Last accessed on July 10, 2020.
28. Clewlow, R. and K. Laberteaux, Shared-use mobility in the United States: Current adoption and potential impacts on travel behavior. In *95th Annual Meeting of the Transportation Research Board (TRB), Washington DC, United States*, 2016.
29. Hsiang, S., D. Allen, S. Annan-Phan, K. Bell, I. Bolliger, T. Chong, H. Druckenmiller, L. Y. Huang, A. Hultgren, E. Krasovich, et al., The effect of large-scale anti-contagion policies on the COVID-19 pandemic. *Nature*, 2020, pp. 1–9.
30. Chowdhury, R., K. Heng, M. S. R. Shawon, G. Goh, D. Okonofua, C. Ochoa-Rosales, V. Gonzalez-Jaramillo, A. Bhuiya, D. Reidpath, S. Prathapan, et al., Dynamic interventions to control COVID-19 pandemic: a multivariate prediction modelling study comparing 16 worldwide countries. *European journal of epidemiology*, Vol. 35, No. 5, 2020, pp. 389–399.
31. Leung, K., J. T. Wu, D. Liu, and G. M. Leung, First-wave COVID-19 transmissibility and severity in China outside Hubei after control measures, and second-wave scenario planning: a modelling impact assessment. *The Lancet*, 2020.

APPENDIX

Derivation of NGM for Spatial SEIR model

To compute the next generation matrix, we actually only care about the *infected subsystem*, the set of populations that contain infected individual consisting of $E_v(t)$ and $I_v(t)$ for all regions $v \in \mathscr{V}$. To compute the Jacobian, we need to compute $\frac{\partial}{\partial E_v}\left(\frac{dE_u}{dt}\right), \frac{\partial}{\partial I_v}\left(\frac{dE_u}{dt}\right), \frac{\partial}{\partial E_v}\left(\frac{dI_u}{dt}\right), \frac{\partial}{\partial I_v}\left(\frac{dI_u}{dt}\right)$, where each is evaluated at $S_u = N_u$ and $I_u = 1$.

Note there exists a disease-free equilibrium with $S_v = N_v$ and $I_v = 0$ for all $v \in \mathscr{V}$. In the case of fixed control, we can directly plug in these values to further simplify the computation. Note both F and Vin dimension $\mathbb{R}^{2|\mathscr{V}|\times 2|\mathscr{V}|}$ and hence we can write the NGM as:

$$G = FV^{-1}|_{>0} \tag{20}$$

$$[F]_{uv} = \begin{cases} p_H\beta_v(1-\alpha) + p_W\sum_{u\in\mathscr{N}^+(v)} r_{vu}^2\beta_u\frac{(1-\alpha)N_v[\rho_N^\intercal N]_u}{([\rho_N^\intercal N]_u-\alpha[\rho_N^\intercal I]_u)^2} + \\ \qquad p_C\sum_{w\in\mathscr{C}^+(v)} x_{vw}r_{vw}^2\beta_w\frac{(1-\alpha)N_v[\rho_C(x)^\intercal C]_w}{([\rho_C(x)^\intercal C]_w-\alpha[\rho_C(x)^\intercal I]_w)^2}, & u = v, u, v \in \mathscr{V} \\ \\ p_W\sum_{w\in\mathscr{N}^+(u)\cap\mathscr{N}^+(v)}\beta_w r_{uw}r_{vw}\frac{(1-\alpha)N_v[\rho_N^\intercal N]_w}{([\rho_N^\intercal N]_w-\alpha[\rho_N^\intercal I]_w)^2} + \\ \qquad p_C\sum_{w\in\mathscr{C}^+(u)\cap\mathscr{C}^+(v)}\beta_w r_{uw}r_{vw}\frac{(1-\alpha)N_v[\rho_C(x)C]_w}{([\rho_C(x)^\intercal C]_w-\alpha[\rho_C(x)^\intercal I]_w)^2}, & u \neq v, u, v \in \mathscr{V} \end{cases}, \tag{21}$$

$$V = \begin{bmatrix} \frac{1}{\delta} & \cdots & 0 & 0 & \cdots & 0 \\ \vdots & \ddots & \vdots & \vdots & \ddots & \vdots \\ 0 & \cdots & \frac{1}{\delta} & 0 & \cdots & 0 \\ \frac{1}{\delta} & \cdots & 0 & \gamma & \cdots & 0 \\ \vdots & \ddots & \vdots & \vdots & \ddots & \vdots \\ 0 & \cdots & \frac{1}{\delta} & 0 & \cdots & \gamma \end{bmatrix}. \tag{22}$$

If we compute the expanded G from these expression for F and V^{-1} we get

$$G = FV^{-1}|_{>0} = \begin{bmatrix} 0 & \cdots & 0 & \frac{1}{\gamma}[F]_{E_vI_v} & \cdots & \frac{1}{\gamma}[F]_{E_uI_v} \\ \vdots & \ddots & \vdots & \vdots & \ddots & \vdots \\ 0 & \cdots & 0 & \frac{1}{\gamma}[F]_{E_uI_v} & \cdots & \frac{1}{\gamma}[F]_{E_vI_v} \\ 0 & \cdots & 0 & 0 & \cdots & 0 \\ \vdots & \ddots & \vdots & \vdots & \ddots & \vdots \\ 0 & \cdots & 0 & 0 & \cdots & 0 \end{bmatrix}|_{>0} \tag{23}$$

and here the nonzero submatrix is the NGM, G. We can see that:

$$[G]_{vv} = \frac{1}{\gamma}[F]_{E_vI_v} \tag{24}$$

$$[G]_{vu} = \frac{1}{\gamma}[F]_{E_uI_v} \tag{25}$$

Commute networks in numerical experiments

In the simulation, we use the following commute networks ($|\mathscr{V}_{HW}| = 4, |\mathscr{V}_C| = 6$) with randomly generated population (with expected total population of 100) and route choice.

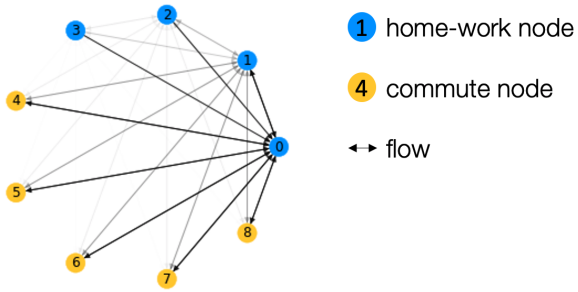

FIGURE 13: Commute network for control policy validation

The route-based control policy for the adaptive flow control numerical experiments are shown in Figure 14.

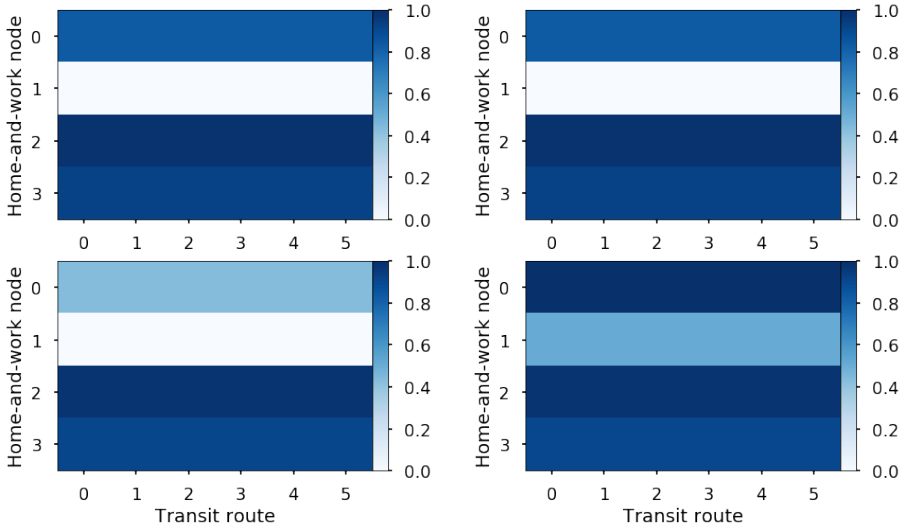

(a) At $t = 0$ (up) with $\kappa(0) = 0.5$ and $t' > 0$ (down) with $\kappa(t') = 0.2$.

(b) At $t = 0$ (up) with $\kappa(0) = 0.5$ and $t' > 0$ (down) with $\kappa(t') = 0.9$.

FIGURE 14: Optimal transit flow control $\boldsymbol{x}^*(t)$ with different strictness of health measures

The connectivity of the public transit is required for reconstructing the commute network in NYC case study. Considering that the physical public transit lines are not an appropriate unit for commuting route choice as passengers may transfer between lines in a single trip and thus causing contagion on all visited lines. By limiting the number of transfer to one, we can crawling the public transit data (*27*) to reconstruct the commute network transfer graph in Figure 15.

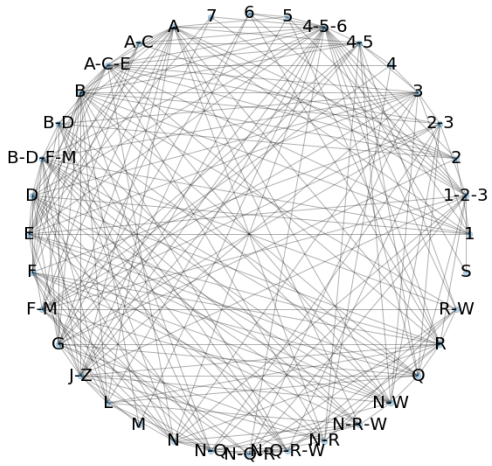

FIGURE 15: Connectivity of the MTA subway systems; Each edge in the graph is $v \in \mathscr{V}_C$ in the commute network